Dipole Cancellation as an Artifact Suppression Technique in Simultaneous Electrocorticography Stimulation and Recording

Jeffrey Lim[1], Po T. Wang[1], Haoran Pu[2], Charles Y. Liu[3], Spencer Kellis[3,4], Richard A. Andersen[4], Payam Heydari[2], An H. Do[5], and Zoran Nenadic[1,2]

***Abstract*— Fully-implantable, bi-directional brain-computer interfaces (BCIs) necessitate simultaneous cortical recording and stimulation. This is challenging since electrostimulation of cortical tissue typically causes strong artifacts that may saturate ultra-low power (ULP) analog front-ends of fully-implantable BCIs. To address this problem, we propose an efficient hardware-based method for artifact suppression that employs an auxiliary stimulator with polarity opposite to that of the primary stimulator. The feasibility of this method was explored first in simulations, and then experimentally with brain phantom tissue and electrocorticogram (ECoG) electrode grids. We find that the canceling stimulator can reduce stimulation artifacts below the saturation limit of a typical ULP front-end, while delivering only ∼10% of the primary stimulator's voltage.**

I. Introduction

Electrocorticography (ECoG) is a promising brain-computer interface (BCI) platform for restoring motor function to individuals with severe paralysis [1], [2]. Normally, these BCIs exploit visual feedback to achieve closed-loop operation, which is suboptimal for movement restoration where persistent somatosensory feedback is crucial. Recent human studies [3], [4] used subdurally implanted ECoG grids to elicit somatosensation via cortical electrostimulation, suggesting that future ECoG-based BCIs should be able to restore both motor and sensory functions. These "bi-directional" BCIs will operate in a more biomimetic fashion, and their performance and ease-of-use would likely improve upon the present-day BCIs [5]. Additionally, ECoG-based bi-directional BCIs could be realized as fully-implantable systems, which would greatly improve their utility [6], [7].

A major technical challenge to developing a fully-implantable, ECoG-based, bi-directional BCI is the presence of strong artifacts created by cortical stimulation. Specifically, a fully-implantable BCI must operate in an ultra-low-power (ULP) regime, which limits the nominal supply voltage of its analog front-end [7]. If stimulation artifacts reach or exceed this voltage—a likely scenario in bi-directional BCI operation—recording amplifiers will be saturated, thereby leading to unrecoverable loss of data.

Supported by National Science Foundation (Award # 1446908, 1646275)

[1]Dept. of Biomedical Engineering, University of California Irvine (UCI), Irvine, CA 92697, {limj4,ptwang,znenadic}@uci.edu

[2]Dept. of Electrical Engineering and Computer Science, UCI, Irvine, CA 92697, {haoranp1,payam}@uci.edu

[3]Dept. of Neurological Surgery, University of Southern California, Los Angeles, CA 90033, cliu@usc.edu

[4]Div. of Biology and Biological Engineering, CALTECH, Pasadena, CA 91125, {skellis,andersen}@vis.caltech.edu

[5]Dept. of Neurology, UCI, Irvine, CA 92697, and@uci.edu

A simple approach to mitigating amplifier saturation is blanking [8], wherein recording is turned off during stimulation. This strategy compromises the BCI performance and is inadequate for applications that require continuous feedback. Studies [6], [7] have proposed reducing artifacts by placing the stimulating and recording channels in a specific spatial configuration, followed by filtering at the front-end. This approach, however, imposes severe electrode placement constraints, which may be difficult to satisfy in a multielectrode setting. In addition, the spectra of neural signals and artifacts tend to overlap [9], which limits the effectiveness of filtering. Mendrela et al. [10] proposed an adaptive filtering approach that estimates the "transfer function" of the stimulation-recording path, and in turn the artifact component of the recorded signal. This component is then subtracted at the front-end, before the signal is amplified. While encouraging, this method does not scale favorably with the number of electrodes and assumes that the artifact transmission path is a linear time-invariant system.

We propose an alternative artifact suppression method that is based on auxiliary stimulation applied between the stimulation and recording sites. This secondary stimulation is delivered simultaneously and in opposite polarity to the primary stimulation. Also, it operates at a fraction of the primary stimulation amplitude. We demonstrate the feasibility of this method first in simulations, and then in benchtop experiments with ECoG electrodes and phantom tissue. Our results indicate that the artifacts can be suppressed below the potential saturation limit of an ULP amplifier array, while operating at only ∼10% of the stimulation voltage and without significant interference with the primary stimulation.

II. Methods

A. Motivation

To motivate the development of our method, we observe that the artifact amplitude decays with the distance from a stimulation point. For simplicity, assume that stimulation is delivered at a point $r = 0$ (see Fig. 1), and that the stimulation voltage is given by: $V_{\text{stim}}(r) = 1/(r + r_0)$, where $r_0 > 0$ is a constant. Note that this model corresponds to a monopolar current source [11] with normalized values of the current amplitude and conductivity. As can be seen, the artifacts exceed a hypothetical saturation threshold, V_{th}, in the assumed recording region. We then introduce a sink at $r = r_c$ with voltage $V_{\text{canc}}(r) = -\alpha/(|r - r_c| + r_0)$, where $\alpha \in [0, 1]$ is a fraction of the original source current. By simultaneously activating stimulation and cancellation, the

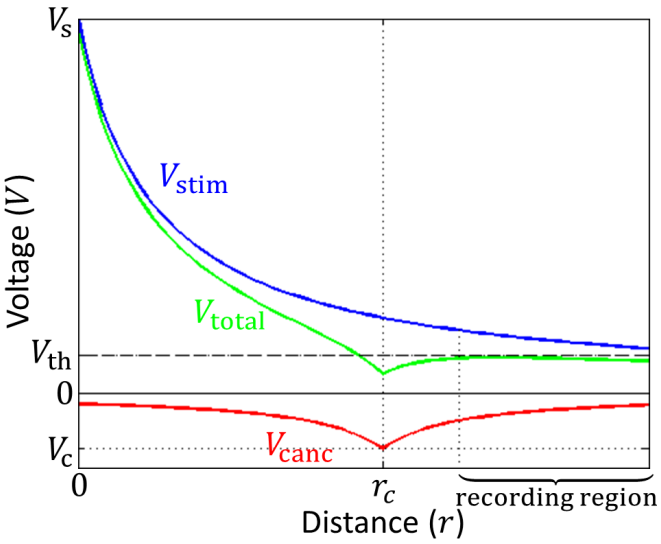

Fig. 1. The voltage profile V_{stim} (blue) due to monopolar stimulation delivered at $r = 0$. V_{th}–saturation threshold. Recording electrodes are assumed to be on the far right. Canceling (opposite) stimulation at $r = r_c$ with the voltage profile V_{canc} (red). $V_{total} = V_{stim} + V_{canc}$ (green), with $V_c = -0.15V_s$.

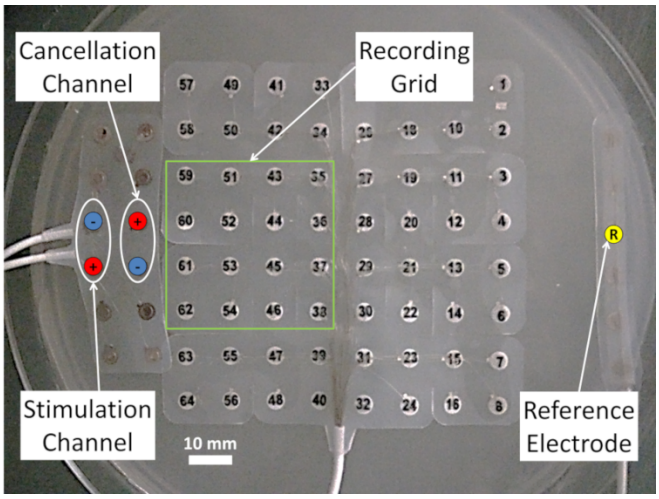

Fig. 2. ECoG grids placed over phantom tissue in a Petri dish. The primary stimulation channel is located on the 2×6 grid on the pair farthest from the 8×8 recording grid. The cancellation channel is placed between the stimulation channel and the recording grid. The reference electrode is chosen from a 1×6 strip, positioned away from the stimulation channel.

voltages are superimposed: $V_{total} = V_{stim} + V_{canc}$. Choosing an appropriate α, e.g., $\alpha = 0.15$, renders $V_{total}(r) < V_{th}$ over the recording region, thus preventing saturation. At the same time, since $V_{total}(0) \approx V_{stim}(0) = V_s$, introducing cancellation does not significantly interfere with stimulation at $r = 0$. This concept, extended to bipolar stimulation, is the basis of our approach.

B. Simulations

Voltage propagation due to bipolar electrical stimulation is more appropriately described with the dipole model:

$$V_s(x,y,t) = \frac{I(t)}{4\pi\sigma}\left[\frac{1}{r_s^+(x,y)} - \frac{1}{r_s^-(x,y)}\right] \quad (1)$$

where $V_s(x,y,t)$ is the voltage at a position (x,y) and time t, I is the stimulation current, σ (S/m) is the bulk tissue conductivity, and $r_s^+$and r_s^- are the distances between the point (x,y) and the dipole source and sink, respectively. Since subdurally implanted ECoG grids are primarily planar, the model (1) is set up in 2D (extension to 3D is straightforward). Also, this model assumes a primarily resistive signal propagation mechanism through an isotropic homogeneous medium. This is in agreement with our recent study [9], which characterized the artifact propagation in the human brain based on clinically recorded ECoG data.

Similar to (1), the canceling dipole can be modeled as:

$$V_c(x,y,t) = -\alpha\frac{I(t)}{4\pi\sigma}\left[\frac{1}{r_c^+(x,y)} - \frac{1}{r_c^-(x,y)}\right] \quad (2)$$

where, as before, $\alpha \in [0, 1]$, and $r_c^+$and r_c^- are the distances between the point (x,y) and the canceling dipole source and sink, respectively. When cancellation is turned on, the total voltage is obtained by superposition: $V_t(x,y,t) = V_s(x,y,t) + V_c(x,y,t)$. These voltages were then simulated for a typical stimulation-recording ECoG grid configuration.

Since cancellation can potentially interfere with stimulation, we also simulated its effect on the voltage distribution near the stimulating dipole. To quantify the voltage discrepancy due to the presence of cancellation, we calculated $V_t(x,y,t) - V_s(x,y,t)$, which is essentially just $V_c(x,y,t)$. We are especially interested in $V_c(x_s^+, y_s^+, t)$ and $V_c(x_s^-, y_s^-, t)$, where (x_s^+, y_s^+) and (x_s^-, y_s^-) are the locations of the stimulation source and sink, respectively. If these voltages are sufficiently large, they may interfere with the stimulation's ability to cause sensation. We will refer to this phenomenon as desensitization throughout this paper.

C. Phantom Tissue Experiments

Food-grade agar (Now Foods, Bloomingdale, IL) was mixed into boiling water to form a gel preparation, which was poured into a Petri dish and an open-ended cylindrical mold. Both were placed in a refrigerator to set overnight. The voltage and current were measured across the gel within the mold, and the conductivity was calculated based on the radius and length of the mold. The conductivity of agar gels is typically manipulated by NaCl doping [12], in order to achieve brain conductivity values. However, the gel used in our study achieved these values without the doping.

ECoG grids (Ad-Tech, Oak Creek, WI) with platinum contacts were placed onto the agar phantom for recording and stimulating purposes (see Fig. 2). The grids were soaked with deionized water and downward pressure was applied to ensure contact with the gel. Due to a limited number of amplifiers in our recording system, a 4×4 subset of an 8×8 grid was designated as the recording grid. A 2×6 grid was used for stimulation, and electrode pairs were chosen to deliver bipolar stimulation and cancellation as shown in Fig. 2. A 1×6 ECoG strip was placed on the far end (away from the stimulation channel), and one of its central electrodes was used as the reference. The leads of

the recording grid and reference were then connected to an array of bioamplifiers (MP150/EEG100C, Biopac Systems, Inc., Goleta, CA) where signals were amplified (×5,000) and acquired at 4 kHz.

A function generator (33250A, Agilent Technologies, Santa Clara, CA) supplied voltage to the bipolar stimulation channel (Fig. 2). Cancellation was achieved by connecting a second function generator to the cancellation channel while reversing the polarity. The two function generators were synchronized and programmed to emit a 50-Hz sine wave for 2 s. The stimulation voltage peak-to-peak amplitude was held at 100 mV, while the cancellation voltage was swept from 0 mV to 100 mV in 10-mV increments (0%-100% cancellation). For each cancellation level, ten trials of 2-s stimulation trains were completed, and the signals from 16 ECoG electrodes were recorded and stored.

D. Analysis

The 2-s stimulation epochs were segmented from the raw data. For each epoch, the individual peaks/troughs were detected for all 16 channels and their median values were calculated across the epoch. For each recording electrode, the overall artifact amplitude was then obtained by calculating the median of these values across 10 trials. This procedure was repeated at each cancellation level, and the values were spatially interpolated, color-coded, and mapped for analysis.

This analysis was facilitated by defining a hypothetical ULP amplifier saturation region based on an implantable bi-directional BCI prototype [7]. Specifically, given a supply voltage of 2.2 V and a gain of 66 dB, the saturation limit for this amplifier is $\pm 1100\ \mu$V. The effectiveness of our method was then gauged by superimposing the saturation contours onto the artifact spatial distribution maps.

E. Control Experiments

To investigate whether cancellation has a significant desensitization effect, the stimulation channel was disconnected while the cancellation channel was turned on. Signals were then recorded from the two ECoG electrodes previously used as the stimulation channel. Note that this is equivalent to simulating $V_c(x_s^+, y_s^+, t)$ and $V_c(x_s^-, y_s^-, t)$ in Section II-B. The recording set up was otherwise the same as in the previous experiment. These measurements were performed by sweeping the peak-to-peak cancellation voltage from 10 mV to 100 mV in 10-mV increments, thus mimicking various cancellation levels. The recorded data were then analyzed as in Section II-D, and the desensitization voltages, defined as the total voltage swing across the two electrodes, were calculated. These values were then tabulated and compared to the voltage swings caused by the stimulator. Since it is not possible to measure the voltages directly beneath the stimulating electrodes, these voltage swings, referred to as V_{gel}, were estimated by modeling the electrode-gel interface.

III. Results

A. Simulation Results

Two dimensional voltage fields were simulated as described in Section II-B. To this end, the stimulating and recording ECoG grids were assumed to be adjacent to each other (see Fig. 3), so as to mimic their respective placement on the sensory and motor cortices. The conductivity $\sigma = 1.7$ S/m was chosen to match the physiological values of human cerebrospinal fluid (CSF) [13]. Note that due to a subdural placement of ECoG electrodes, most of the current will pass through the subarachnoid space, meaning that the bulk conductivity is dominated by that of CSF. Since (1) and (2) are static models, the current $I(t)$ was assumed constant, and the amplitude $I = 2.1$ mA was chosen. This caused the saturation of 4 channels of the recording grid (Fig. 3A).

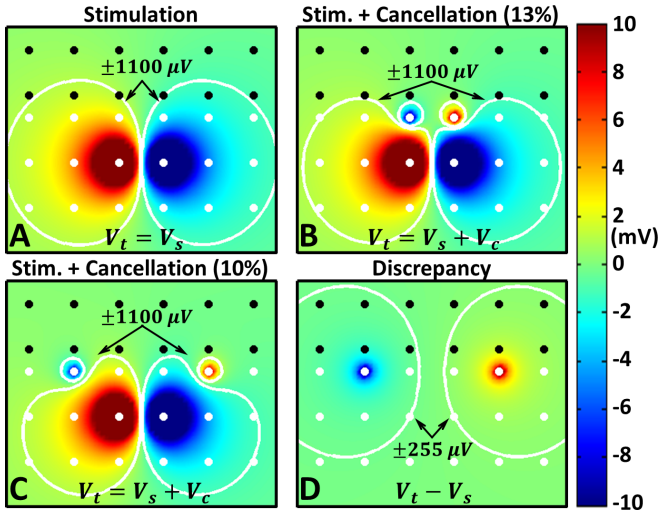

Fig. 3. Simulation results. A: Spatial distribution of voltage due to the stimulating dipole located in the middle of the stimulating grid (white dots). The electrode pitch is 10 mm. The recording grid (black dots) cannot sense the voltages within the saturation contour. B: The voltage field after turning on the canceling dipole with $\alpha = 0.13$. The saturation contour is reshaped away from the recording grid. C: An alternative location of the canceling dipole ($\alpha = 0.10$). D: The discrepancy between the canceled field (C) and the original field (A). The voltages above 10 mV (below -10 mV) are clipped.

Fig. 3B shows the effect of cancellation obtained by turning on the canceling dipole (parallel and oppositely polarized to the stimulating dipole), which was able to reshape the saturation contour and move it away from the recording grid, while drawing only 13% of the stimulating dipole current. The value $\alpha = 0.13$ was determined by trial and error to merely demonstrate our method. In a more rigorous approach, the calculation of this parameter could be cast within a constrained optimization framework. Fig. 3C shows that the choice of the canceling dipole is not unique; in particular, this solution is superior to the previous one since the canceling dipole draws even less current and the saturation contours are farther from the recording grid. The location/orientation of the canceling dipole could also be found through optimization.

Fig. 3D illustrates the discrepancy between the voltage fields in Figs. 3C and 3A. The discrepancy at the location of the stimulating dipole is 255 μV—a value significantly below the voltage delivered by the stimulator. Therefore, these small field perturbations in the vicinity of the stimulating dipole are unlikely to cause desensitization.

TABLE I

VOLTAGES DUE TO CANCELLATION, V_c^- AND V_c^+, MEASURED AT THE STIMULATION CHANNEL'S SINK AND SOURCE, RESPECTIVELY.

Peak-to-peak Cancellation Voltage (mV)	V_c^- (mV)	V_c^+ (mV)	Desensitization Voltage $V_d = V_c^- - V_c^+$ (mV)	$\frac{V_d}{V_{\text{gel}}}$ (%)
10	0.2586	-0.1390	0.3976	1.7
20	0.4562	-0.3477	0.8039	3.4
30	0.6575	-0.5513	1.2088	5.1
40	0.8609	-0.7561	1.6170	6.9
50	1.0623	-0.9571	2.0194	8.6
60	1.2623	-1.1574	2.4197	10.3
70	1.4612	-1.3522	2.8134	11.9
80	1.6590	-1.5486	3.2076	13.6
90	1.8064	-1.7372	3.5436	15.0
100	1.8923	-1.9181	3.8104	16.2

B. Experimental Results

By measuring the voltage and current across the mold filled with phantom tissue (see Section II-C), the conductivity of the gel was estimated to be 1.5 S/m, which is consistent with the conductivity of human CSF [12]. Experimentally recorded data were then analyzed as outlined in Section II-D. The 50-Hz stimulation artifacts were clearly visible on all 16 channels, and depending on the electrode location, the phase shifts were either 0° or 180°. Fig. 4 shows the evolution of the stimulation artifact spatial maps at varying levels of cancellation. At 0% (the cancellation channel off), 3 recording electrodes fall within the saturation region. At 10%, the saturation contour recedes with only a single electrode remaining in the saturation region. When cancellation is at 20%, all the artifact amplitudes are below the saturation level, and they continue to decrease up until 40% cancellation level. From this point, the artifact amplitudes begin to increase, as the canceling channel becomes the dominant source of artifacts due to its proximity to the recording grid. This also leads to the reversal of the field's polarity. Finally, at 100% cancellation level, the saturation contour re-emerges with two channels falling within the saturation region.

The control experiment data were then analyzed as outlined in Section II-E. For each cancellation level from 10% to 100%, the median voltages at the two electrodes corresponding to the stimulation channel were calculated, and the results are shown in Table I. Note that the voltage measured at the electrode corresponding to the stimulator sink, V_c^-, is positive. This is expected behavior, given that this electrode is closer to the source of the cancellation channel (Fig. 2). Similarly, the voltage V_c^+ is negative. The desensitization voltage, V_d, defined as the voltage swing across these electrodes, ranged from 0.4 mV at 10% cancellation to 3.8 mV at 100% cancellation.

To gauge the likelihood of desensitization, V_d was compared to the stimulation voltage "experienced" by the gel. This voltage, denoted by V_{gel}, could not be directly measured, and had to be estimated. To this end, the electrode-gel interface was modeled as an RC circuit (see Fig. 5):

$$|V_{\text{gel}}| \triangleq |V_1 - V_2| = \frac{R}{|2Z+R|}|V_s| \tag{3}$$

where Z is the impedance of the electrode-gel contact, R is the resistance of the gel current path, and $|V_s| = 100$ mV. Based on commonly reported values for ECoG electrodes [14], the total impedance of the path is assumed to be: $|2Z+R| = 1000\ \Omega$. The resistance, R, was calculated based on the gel conductivity, σ, the distance between the electrodes (10 mm), and assuming a cylindrical current path with a diameter equal to the depth of the gel (6 mm):

$$R = \frac{L}{\sigma A} = \frac{10\times10^{-3}\,\text{m}}{1.5\,\frac{\text{S}}{\text{m}}\,\pi(3\times10^{-3}\,\text{m})^2} = 235.8\,\Omega \tag{4}$$

After substituting these values into (3), we find: $|V_{\text{gel}}| = 23.58$ mV. The ratio V_d/V_{gel} was then calculated (Table I). At cancellation levels between 10% and 20%, which are sufficient to prevent saturation, the desensitization voltage is only a small fraction ($< 3.4\%$) of the gel voltage and is therefore unlikely to interfere with stimulation.

IV. DISCUSSION

Our simulation and benchtop experiments demonstrate that it is possible to shield recording electrodes from excessive artifact contamination by applying an auxiliary canceling dipole located between the stimulating dipole and the recording grid. Our method essentially amounts to quadrupole stimulation, where the two dipoles are asymmetric, though charge-balanced. Unlike competing artifact suppression methods, e.g. [10], our method's primary objective is not to eliminate stimulation artifacts, but rather to keep them below the saturation limit of a ULP analog front-end. The remaining artifacts can be efficiently removed using a variety of digital signal processing techniques [16].

Our preliminary results indicate that saturation can be prevented by the canceling dipole drawing only $\sim$10% of the stimulating dipole's current. Therefore, the power overhead of this additional dipole is relatively small. Our analysis also suggests that the canceling dipole does not significantly interfere with the primary stimulation and is therefore unlikely to cause desensitization. In addition, since it operates at a fraction of the stimulation dipole's amplitude, the canceling dipole by itself is unlikely to cause sensation. These claims, however, can only be verified empirically by experimenting with human subjects, and the simple calculations in this study can provide useful guidelines.

While this study is primarily concerned with ECoG electrodes, our method may be applicable to other recording/stimulation modalities, such as microelectrode arrays [5], [17]. The main weakness of our method is that it requires electrodes between the stimulation and recording sites. This concern is substantially mitigated by employing high-density ECoG grids [18].

The canceling dipole amplitude and position were chosen to simply demonstrate and experimentally validate our method. These parameters could be optimized which would

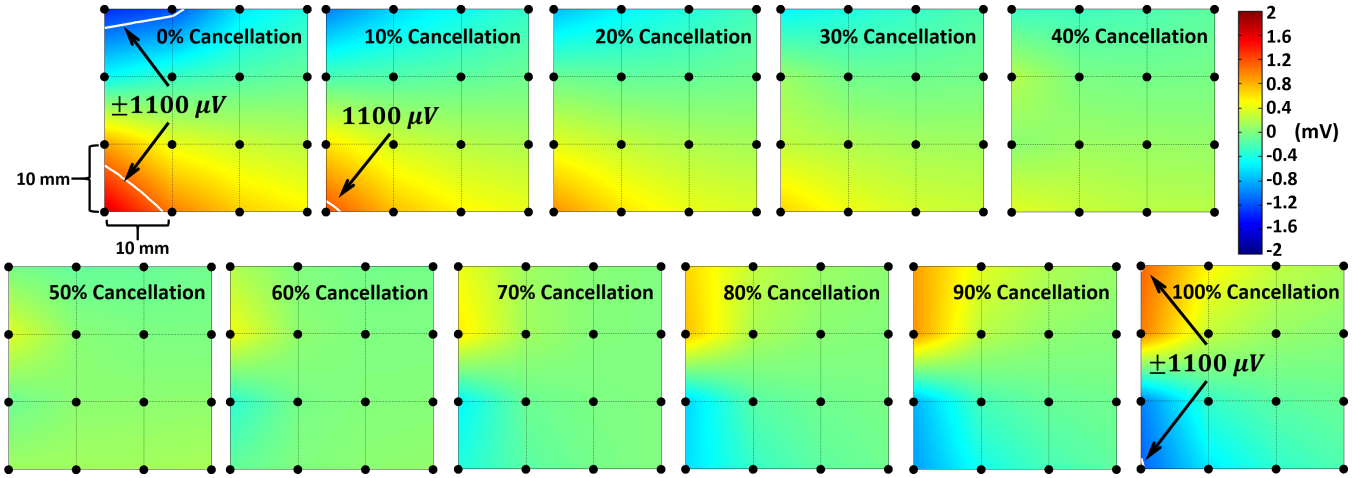

Fig. 4. Artifact spatial distribution maps for varying levels of cancellation from 0% to 100%. The maps are oriented in the same way as the recording grid in Fig. 2, with black dots representing individual electrodes. Cancellation levels between 10% and 20% are sufficient to prevent saturation.

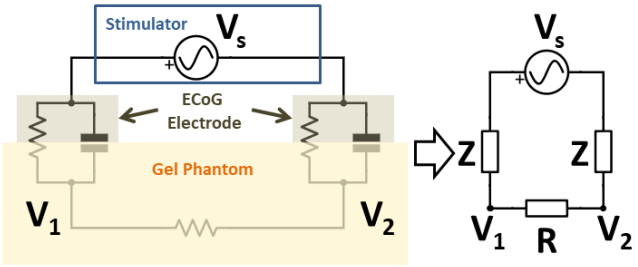

Fig. 5. Model of the gel-electrode interface [15]. The stimulator is an AC voltage source with an amplitude, V_s. The gel was assumed to be purely resistive with some resistance R. V_{gel} is the voltage across this resistor.

result in a greater degree of artifact suppression. Factors such as power consumption and desensitization voltage could be used as constraints in this optimization process. The development of such an optimization framework is beyond the scope of this study and will be pursued in the future.

References

[1] W Wang, JL Collinger, AD Degenhart, EC Tyler-Kabara, AB Schwartz, DW Moran, DJ Weber, B Wodlinger, RK Vinjamuri, RC Ashmore, et al. An electrocorticographic brain interface in an individual with tetraplegia. *PLOS One*, 8(2):e55344, 2013.

[2] MJ Vansteensel, EG Pels, MG Bleichner, MP Branco, T Denison, ZV Freudenburg, P Gosselaar, S Leinders, TH Ottens, MA Van Den Boom, et al. Fully implanted brain–computer interface in a locked-in patient with ALS. *New Engl. J. Med.*, 375(21):2060–2066, 2016.

[3] SV Hiremath, EC Tyler-Kabara, JJ Wheeler, DW Moran, RA Gaunt, JL Collinger, ST Foldes, DJ Weber, W Chen, ML Boninger, et al. Human perception of electrical stimulation on the surface of somatosensory cortex. *PLOS One*, 12(5):e0176020, 2017.

[4] B Lee, D Kramer, MA Salas, S Kellis, D Brown, T Dobreva, C Klaes, C Heck, C Liu, and RA Andersen. Engineering artificial somatosensation through cortical stimulation in humans. *Front. Syst. Neurosci.*, 12(24), 2018.

[5] S Flesher, J Downey, J Collinger, S Foldes, J Weiss, E Tyler-Kabara, S Bensmaia, A Schwartz, M Boninger, and R Gaunt. Intracortical microstimulation as a feedback source for brain-computer interface users. In *Brain-Computer Interface Research*, pages 43–54. Springer, 2017.

[6] S Stanslaski, P Cong, D Carlson, W Santa, R Jensen, G Molnar, WJ Marks, A Shafquat, and T Denison. An implantable bi-directional brain-machine interface system for chronic neuroprosthesis research. In *Proc. 31st Ann. Int. Conf. IEEE EMBS*, pages 5494–5497, 2009.

[7] AG Rouse, SR Stanslaski, P Cong, RM Jensen, P Afshar, D Ullestad, R Gupta, GF Molnar, DW Moran, and TJ Denison. A chronic generalized bi-directional brain–machine interface. *J. Neural Eng.*, 8(3):036018, 2011.

[8] JE O'Doherty, MA Lebedev, PJ Ifft, KZ Zhuang, S Shokur, H Bleuler, and MAL Nicolelis. Active tactile exploration using a brain–machine–brain interface. *Nature*, 479(7372):228, 2011.

[9] J Lim, PT Wang, AK Bidhendi, OM Arasteh, SJ Shaw, M Armacost, H Gong, CY Liu, P Heydari, AH Do, et al. Characterization of stimulation artifact behavior in simultaneous electrocorticography grid stimulation and recording. In *Proc. 40th Ann. Int. Conf. IEEE EMBS*, pages 4748–4751, 2018.

[10] AE Mendrela, J Cho, JA Fredenburg, V Nagaraj, TI Netoff, MP Flynn, and E Yoon. A bidirectional neural interface circuit with active stimulation artifact cancellation and cross-channel common-mode noise suppression. *IEEE J. Solid-St. Circ.*, 51(4):955–965, 2016.

[11] CW Lee, H Dang, and Z Nenadic. An efficient algorithm for current source localization with tetrodes. In *Proc. 29th Ann. Int. Conf. IEEE EMBS*, pages 1282–1285, 2007.

[12] MA Kandadai, JL Raymond, and GJ Shaw. Comparison of electrical conductivities of various brain phantom gels: Developing a 'brain gel model'. *Mater. Sci. Eng. C*, 32(8):2664–2667, 2012.

[13] J Latikka and H Eskola. The electrical conductivity of human cerebrospinal fluid in vivo. In *World Congress on Medical Physics and Biomedical Engineering 2018*, pages 773–776. Springer, 2019.

[14] KA Sillay, P Rutecki, K Cicora, G Worrell, J Drazkowski, JJ Shih, AD Sharan, MJ Morrell, J Williams, and B Wingeier. Long-term measurement of impedance in chronically implanted depth and subdural electrodes during responsive neurostimulation in humans. *Brain stimulation*, 6(5):718–726, 2013.

[15] MR Neuman. Biopotential electrodes. In JG Webster, editor, *Medical Instrumentation Application and Design*, chapter 5, pages 183–232. John Wiley & Sons, Inc, New York, NY, 1998.

[16] PT Wang, CM McCrimmon, P. Heydari, AH Do, and Z Nenadic. Subspace-based suppression of cortical stimulation artifacts. In *Proc. 40th Ann. Int. Conf. IEEE EMBS*, pages 2426–2429, 2018.

[17] MA Salas, L Bashford, S Kellis, M Jafari, H Jo, D Kramer, K Shanfield, K Pejsa, B Lee, CY Liu, et al. Proprioceptive and cutaneous sensations in humans elicited by intracortical microstimulation. *eLife*, 7:e32904, 2018.

[18] PT Wang, CE King, CM McCrimmon, JJ Lin, M Sazgar, FPK Hsu, SJ Shaw, DE Millet, LA Chui, CY Liu, et al. Comparison of decoding resolution of standard and high-density electrocorticogram electrodes. *J. Neural Eng.*, 13(2):026016, 2016.